Journal of Korean Powder Metallurgy Institute
Vol. 4, No. 3, 1997

P M 리 뷰

# Processing and Mechanical Behavior of Oxide Based Nanocomposites

**Y. H. Choa, A. Nakahira, T. Sekino and K. Niihara**
*The Institute of Scientific and Industrial Research, Osaka University*
*8-1 Mihogahoka, Ibaraki-shi, Osaka 567, Japan*

## 1. Introduction

In the engineering application, there is a great need for structural materials capable of withstanding both severe environments and high temperatures. $Al_2O_3$ and MgO ceramics are thus of considerable interest, because of their desirable properties including high refractoriness, excellent resistance for oxidation and corrosion and good hardness. These oxide ceramics, however, suffer from relatively low fracture toughness and strength, significant strength degradation at high temperatures and poor thermal shock fracture resistance. Thus, many attempts have been made to improve these problems of $Al_2O_3$ and MgO ceramics by composite technology.[1-11] Structural ceramic composites can be divided into some categories as shown in Table I: microcomposites and several types of nanocomposites [12]. In the microcomposites, the second phase micrometer-size dispersions such as particulate, platelets, whiskers and fibers are dispersed at the grain boundaries of the matrix, while in the nanocomposites, the second phase nanometer size dispersions such as particulate and whisker are incorporated within the matrix grains.

The $ZrO_2$ dispersion is observed to improve remarkably the fracture toughness and strength of $Al_2O_3$ due to its stress-induced transformation.[2,3] The significant increases in both fracture toughness and strength of $Al_2O_3$ and MgO are also achieved by incorporating the SiC whiskers.[4-11] However, the $ZrO_2$ reinforced composites show the strength degradation at relatively low temperature, while, the SiC-whisker reinforced composites are difficult to prepare the dense materials, and displayed relatively lower fracture strength due to whisker, in itself, as fracture origin. These composites could be classified as microcomposites, in which the micro-size dispersions are predominantly located at the grain boundaries of matrix grains, and the improvement of above-mentioned problems by making this type of composites is not sufficient.

To overcome these problems at the same time, thus, we have been studying the ceramic based nanocomposite is one of the particulate reinforced composites, in which the nano-sized particulate is dispersed within the matrix grains and/or at the grain boundaries. Recently, various kinds of ceramic based nanocomposites in the ceramic/ceramic,[12-23] ceramic/metal[24-28] and intermetallic/ceramic[29,30] composite systems have been investigated. Of these nanocomposites, the oxide based nanocomposites demonstrated significantly improved mechanical properties even at high temperatures.[12,13,15-23]

In this review, The processing and mechanical properties of $Al_2O_3$-SiC and MgO-SiC nanocomposite system developed by Niihara and his co-workers have been systematically reviewed. At first, we investigate the basic processing route for $Al_2O_3$-SiC and MgO-SiC nanocomposite system, and the dispersion characteristics and its effects on the microstructure of fine SiC particle dispersed nanocomposites in various solvents without deflocculants were studied for the dispersing process, the ball-milling process, drying process, and the SiC distribution of sintered nanocomposites, systematically. Secondly, the room and high temperature mechanical property of nanocomposites are discussed with microstructure. The effect of the nano sized SiC particulate will be

**Table I. Design concept of the structural ceramics**

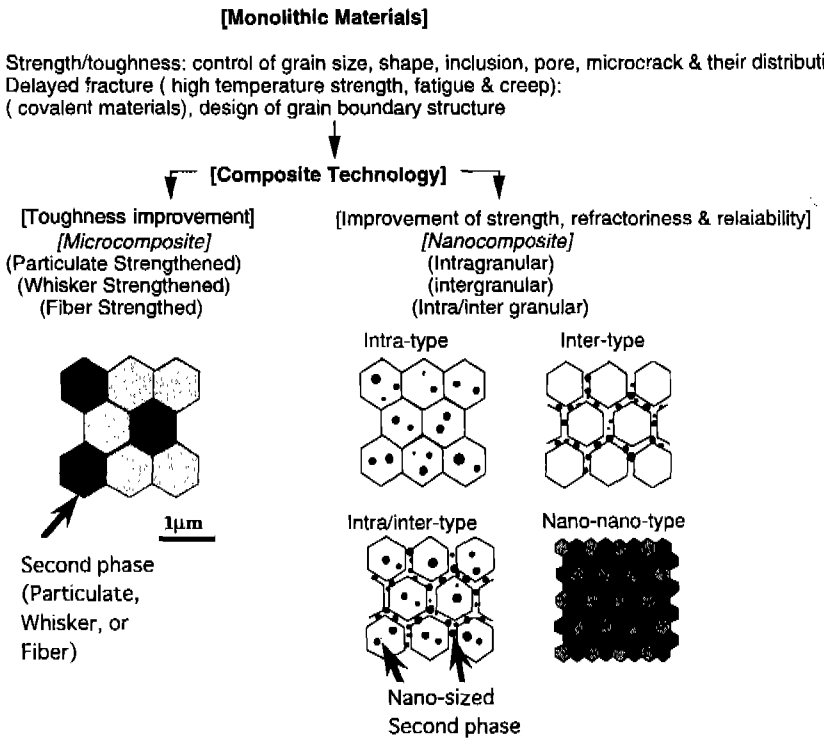


identified not only in strength but also in other mechanical properties including fracture toughness, hardness, creep resistance. As a strengthening and toughening mechanism of ceramic nanocomposites, this paper is focused on a particle bridging or particle pinning mechanism where crack-face shielding arise by the nano-sized particles bridging a propagating crack behind the crack tip. Furthermore, the residual stresses play an important role to strengthen and toughen the oxide materials, then the effects of nano-sized dispersion on residual stresses will be also discussed. Finally, the stress relaxation behavior such as generation of dislocation, dislocation network, and sub-grain boundaries for these nanocomposite systems are investigated by combination of yield stress and residual stress.

Special emphasis is placed on the understanding of nanometer-scale microstructure for improving the mechanical properties for these composites prepared by the conventional powder metallurgical technique.

## 2. Fabrication Processing

Several researcher[31-33,36-41] have been developed the processing to seek a homogeneous dispersion of the SiC nano-reinforcement in oxide matrices for conventional processing which contained the ball-milling without deflocculants, drying, and densification process. There are no reports, however, to understand the dispersibility of SiC particles as well as oxide materials and its effect to microstructure in sintered materials.

Basic conventional processing route for nanocomposite system can be divided into (a) selection of raw powder particles and their dispersion stability, (b) ball-milling process, (c) drying process, and (d) densification process, in various solvents without deflocculants.

### 2.1. Dispersion Test

The following starting raw materials have been used: The highly pure $\gamma$-$Al_2O_3$ powder from Asahi

Chemical Co. with an average particle size of <0.4 μm and SiC powders with an average particle size of 70 nm from Ibiden Co. For MgO-SiC composite mixture, the MgO powder from Ube Industry Ltd. with an average particle size of <0.1 μm and the SiC powder with an average particle size of 100 nm particulate from Mitsui Touatsu Co., were used, respectively. Dispersion properties in the several pure solvents without deflocculants were investigated by sedimentation test. The results of sedimentation tests[42] show significant differences in dispersibility between alcohol and non-alcohol, for MgO and SiC powder. In case of powders dispersed in ethanol, n-butanol and n-hexanol, "very good" dispersion was observed for MgO, SiC, and their mixed powders, being used alcohol solvent. These results are almost coincide with pure SiC dispersibility data reported by Okuyama et al.,[31] except that the better dispersibility was observed in SiC powder for using ethanol and n-butanol compared with that of n-hexanol. These trends of dispersibility also were observed in $Al_2O_3$ and $Al_2O_3$ -SiC mixed powders.

The powders rapidly sedimentated within a few hours when dispersed in n-hexane (non-polar solvent). Generally, both oxide powder and powder with oxide surface layer have hydrophile property, and these powders have no relation with hydrophobic n-hexane, which induce only the Van-der Waals force to enhance the sedimentation.

When the powders dispersed in acetone and alcohols (polar-solvent), hydrogen bonding and steric hindrance could be occurred between the surface of oxide layer and polar-solvents as reported by Kaliszewski and Heuer.[32] They proposed that the deagglomerate mechanism in ethanol are caused by the interaction of ethanol with hydrous $ZrO_2$ powders and steric hindrance as repulsion force. This mechanism can also be applied to dispersion in acetone. In case of the dispersion in acetone, however, rapid sedimentation of dispersed powders was observed, and other authors also reported the same results.[33] Therefore, dispersion property in various solvents can not

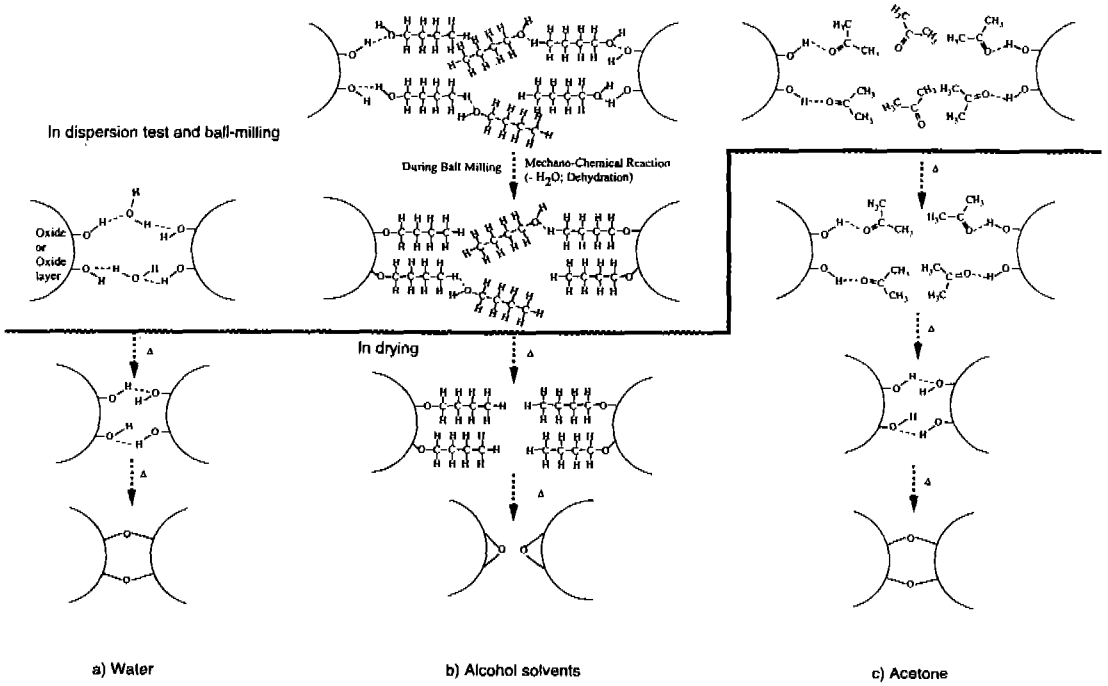


**Fig. 1. Proposed mechanism for dispersion, ball milling, and drying process in (a) water, (b) n-butanol, and (c) acetone. Dotted lines indicate hydrogen bonds.**

explained by only relationship between the hydrogen bond and the steric hindrance.

Both the acetone and the alcohol solvent are formed the hydrogen bond with oxide layer of powder, however, a different hydrogen bond formation process are considered between the acetone and the alcohol. For dispersion in acetone, the hydrogen bond was formed between the oxygen of carbonyl group and hydrogen of hydroxyl group on powder surface, and excess acetone cannot form hydrogen bonds between carbonyl groups on the surface and link particles together, as shown in Fig. 1(c) (commonly, enol- and keto-structure exist together in acetone, but mainly keto-structure without hydroxyl group is stable.[34] Then, only monolayer hydrogen bonding around the particles cannot excess the Van der Waals force as attraction force, and the sedimentation could be occurred, as shown in Table II.

On the other hand, powders dispersed in alcohol behave differently, as shown in Fig. 1(b). Excess alcohol hydrogen bonds to the terminal alkyl groups of the particles, and the chain of alcohol around the particles was formed. Then the agglomerated particles are not formed and good dispersibility could be observed in alcohol, as shown in Table II. Furthermore, because of steric effects, the terminal alkyl groups of the chain of alcohol around the particles also act to prevent close approach of individual particles, while the severe hydrogen bonding of water to among the hydroxyl groups due to high dielectric constant occurs in dispersion at water[32] which induced the formation of agglomerates as shown in Fig. 1(a). The steric effect could be the more effective with the higher carbon number in alcohol, then better dispersibility of particles dispersed in n-hexanol was expected compared with that of ethanol and n-butanol. However, the better dispersibility was observed in SiC powder for using ethanol and n-butanol compared with that of n-hexanol as shown in Table II.

The dielectric constant (ε) of the solvents affects to dispersibility because the surface of ceramic powders such as MgO and SiC powder has high polarity,[35] and when the ceramic powder have a polarity, the powders are stable in polar solvent which means the higher dielectric constant. Comparison of dispersibility with dielectric constant (ε) of the solvents was performed, to see whether high-ε solvents favored stable suspensions, and whether low-ε solvents tended to give rise to flocculation analogous to the work of Mitzuta et al.[36] on silicon powder. No correlation seems to be found for MgO, SiC, and SiC added MgO powders, as shown in Table II; e.g., water and acetone showed poor dispersion characteristics in spite of its higher-ε than that of alcohols. However, as mentioned before, the excess water formed the "strong" hydrogen bond due to higher-ε, and the flocculation were formed. On the other hand, even if the excess acetone cannot form the hydrogen bond between carbonyl groups on the surface and link particles together in acetone, the flocculation were formed, and it is attributed to Van der Waals attraction force. Among alcohol solvents, the excess alcohol

**Table II. Physical properties of solvents and results of dispersion tests**

| Solvents | Dielectrict Constant | Surface Tension ($mN \cdot m^{-1}$) | Viscosity (mPa·s) | D.T. 1 MgO | D.T. 2 MgO | D.T. 1 SiC | D.T. 2 SiC | D.T. 2 MgO/SiC 5 Vol% | D.T. 2 MgO/SiC 20 Vol% |
|---|---|---|---|---|---|---|---|---|---|
| Water | 78.5 | 72.75 | 1.002 | P | F | P | Pc | F | F |
| Acetone | 20.7 | 25.1 | 0.322 | P | F | P | Pb | F | F |
| n-hexane | 1.89 | 18.4 | 0.313 | P | F | P | Pa | F | F |
| Ethanol | 24.3 | 22.4 | 1.20 | VG | Gb | VGa | G | G | G |
| n-butanol | 17.30 | 25.4 | 2.948 | VG | Gc | VGb | G | G | G |
| n-hexanol | 13.2 | 26.2 | – | VG | Ga | G | G | G | G |

D.T. 1; Dispersion Test, for 0.2 g/20 ml, D.T. 2; Dispersion Test, for 5 g/20 ml, S; Sedimentation, F; Flocculated, V. G.; Very Good, G; Good, P; Poor, a<b<c<d<e>f: Sebsequently good dispersibility.

could form the "weak" hydrogen bond compared with water due to lower-ε, and also the steric hindrance acted to deflocculation and deagglomeration. Therefore, it can be proposed that the dispersibility in various solvents would be estimated by thee combination of the formation of hydrogen bonding, dielectric constant, and steric effects, and the optimum condition for dispersibility could be obtained at ethanol and n-butanol.

### 2.2. Wet milling and Drying Process

Fig. 1 shows the schematics of the interaction between the oxide layer around particles and various solvents not only during the dispersion test but also during wet milling, and drying process. During dispersion test, hydrogen bonding and steric hindrance could be occurred between the surface of oxide layer and polar-solvents as mentioned before. However, any mechano-chemical reaction was not promoted even for particles dispersed in alcohols, as shown in Fig. 1(b).

It is considered that hydroxyl groups on the surface of particles would be mechano-chemically reacted only with the terminal hydroxyl groups of alcohol, and this reaction was with dehydration during the ball milling. The mechano-chemical reaction with the dehydration was observed by several researchers[37,38] during the ball milling in alcohol solvents. They reported that the amount of dehydrated water was increased with ball milling time, and mechano-chemical reaction was also observed. For this reaction of alcohol-oxide layers, it could be investigated by TG/DTA analysis.[32,39] Fig. 2(a) and (b) show the TG/DTA results for MgO powder and SiC powder after milled in n-butanol and n-hexane for 24 h and dried at 200℃. The exothermic peak is observed in the DTA patterns for the MgO powder milled in n-butanol. In Fig. 2(b), exothermic reaction was also observed for the SiC powder milled in n-butanol. Notice that the exothermic peaks are at ~280℃ and 330℃ for MgO powder and at 330℃ and 470℃ for SiC powders, respectively. Clearly these are chemical reactions, since they closely correlate with the rate of

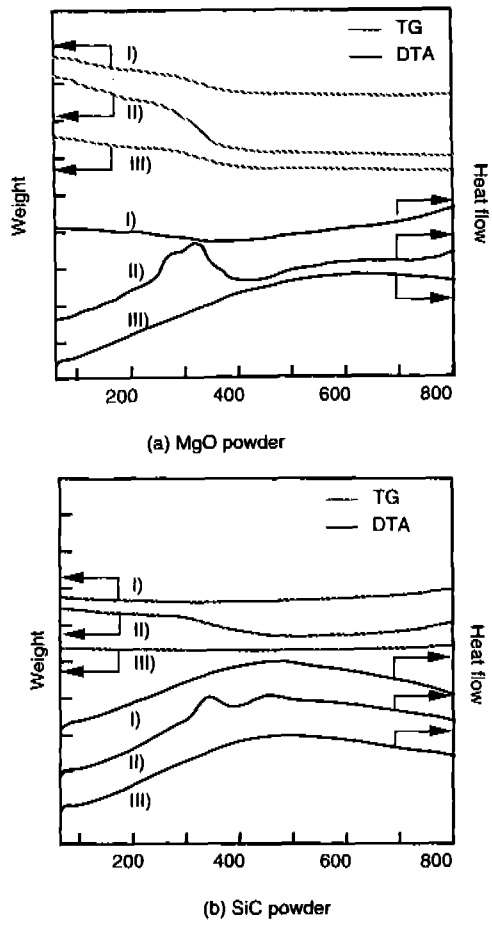


**Fig. 2. TG/DTA patterns for (a) MgO and (b) SiC powders ball-milled in I) as-received powder, II) n-butanol, and III) n-hexane.**

weight loss determined by TG. This chemical reaction, however, was not observed in powders milled in acetone, in spite of polar-solvent. MgO and SiC powders milled in n-hexane for 24 h, also exhibited a quite different DTA patterns which compared with those milled in n-butanol, and the exothermic reactions do not appear in the powder milled in n-hexane as well as those in as-received powders. It is apparent that the reactions involve oxidation of alcohol and dehydration which occurs during ball-milling for using the alcohol solvents, and this exothermic reactions also investigated in $Al_2O_3$ powder.[37,38]

An agglomeration process during the drying was well explained by Kaliszewski and Heuer[32] for hy-

drous $ZrO_2$ powders dispersed in water and ethanol. Fig. 1 suggests how dispersing in water, n-hexane, acetone or alcohol leads to hard and soft agglomerates, respectively. As described in the Lee and Readey,[40] excess water-hydrogen bonds to the terminal hydroxyl groups of the hydrous suspension. In cases where powder particles are in close contact, particle bridging by hydrogen bonding of water to two terminal hydroxyl groups occurs. As drying of the powders commences, these "bridging" water molecules are lost, but the particles are close enough that hydrogen bonding occurs between terminal hydroxyl groups of the different particles. Because of the close proximity of the hydrogen-bonded hydroxyl groups, further dehydration leads to the formation of actual chemical bonds preferentially between powder particles, yielding hard agglomerates. This hard agglomerate induced to form the inhomogeneous microstructure after sintering for $Al_2O_3$ as well as MgO powder, as shown in Fig. 3.

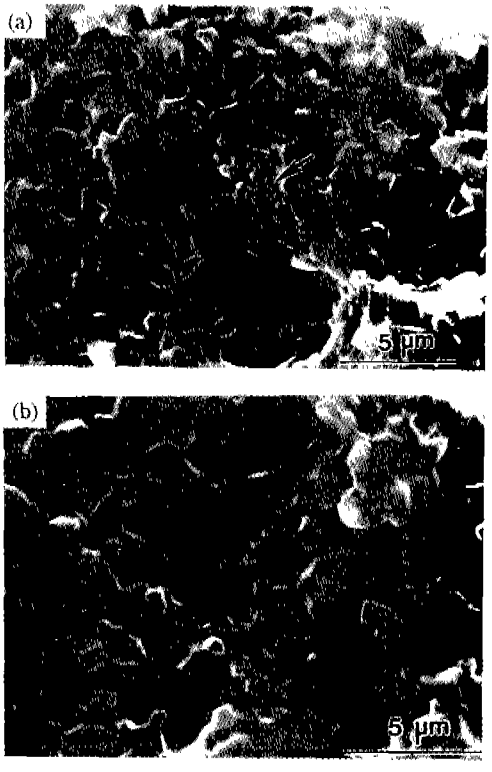


**Fig. 3. SEM micrographs of the fracture surface of $Al_2O_3$ milled in (a) acetone and (b) n-butanol.**

During drying process, the similar agglomerate mechanism are considered for powder particles dispersed in n-hexane and acetone, in spite that the dispersion properties are different among water, n-hexane and acetone in the before drying.

The dispersed powders in n-butanol behave differently, as shown in Fig. 1(b). Excess butanol can form hydrogen bonds between butoxy groups on the surface and links particles together. On continued solvent removal, hydrogen bonding cannot occur between the terminal butoxy groups of different particles. Because of steric effects, the butoxy groups also act to prevent close approach of individual particles. As the drying temperature is increased, removal of the terminal butoxy groups involves a reaction similar to that involved in catalyzed butylene production. Here, two butoxy groups react to form dibuty ether, which rapidly decomposes into two butylene molecules and water.[41] Since close approach of particles is inhibited (relative to those of other solvents), removal of the butoxy groups occurs preferentially between neighboring groups on the same powder particles. Thus, it does not result in chemical bond formation between particles, as in those of other solvents, and formation of hard agglomerates is avoided. Similar beneficial results have been obtained in powders washed with ethanol and 2-propanol.[33] (Removal of ethoxy and isopropoxy groups results in the formation of diethyl ether and propylene, respectively.) Clearly, purely steric effects must be secondary to the control of agglomerate strength in the drying process, while the steric effect affects to dispersibility in dispersion test compared with that in drying process.

Based on the results in this study, the optimum condition of the dispersibility of SiC powders as well as MgO powders is reached by ethanol and n-butanol considering the balance between the steric effects and the dielectric constant of alcohol as well as mechanochemical reaction.

From the SEM observation for thermal etched surface of 5 vol% SiC added MgO based sintered bo-

dies milled in n-butanol and n-hexane,[42] it is considered that SiC particles milled in n-butanol are finer and better distributed than those milled in n-hexane. These results are clearly coincided with particle size distribution measurement data,[42] and well dispersion as well as deagglomeration states obtained at sintered body milled in n n-butanol. Therefore, when $Al_2O_3$-SiC and MgO-SiC composite powders were ball-milled in ethanol or n-butanol, the homogeneous SiC distribution would be obtained.

### 2.3. Sinterability

The densities of composites prepared by conventional processing were strongly dependent on the volume fraction of particulate dispersions and hot-pressing temperature. For the $Al_2O_3$-SiC system, the nearly full densities were achieved at 1,600℃ up to 5 vol% SiC, 1,700℃ for 10 vol% and at 1,800℃ for 20 and 30 vol%. For the MgO-SiC composite, on the other hand, the densities of over 99% were observed for the hot-pressed materials at 1,700 to 1,900℃ depending on the volume fraction of SiC particles.

X-ray diffraction analyses revealed that the $Al_2O_3$ and MgO-SiC composites were composed of only α-$Al_2O_3$ and β-SiC and of only MgO and SiC, respectively, and were free from other impurity phases. The average grain sizes of $Al_2O_3$ and MgO matrices were approximately 2 to 3 μm for the both composites prepared under the conditions above-mentioned.

As shown in Fig. 4, TEM observations indicated

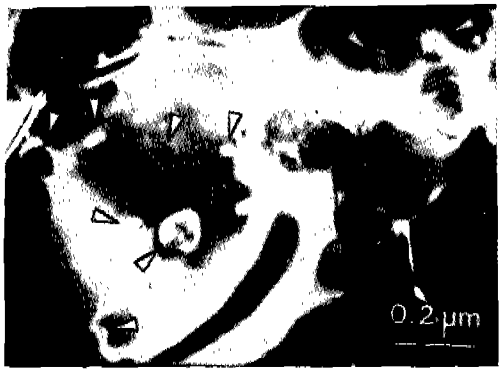


**Fig 4. TEM picture of the $Al_2O_3$-SiC nanocomposite.**

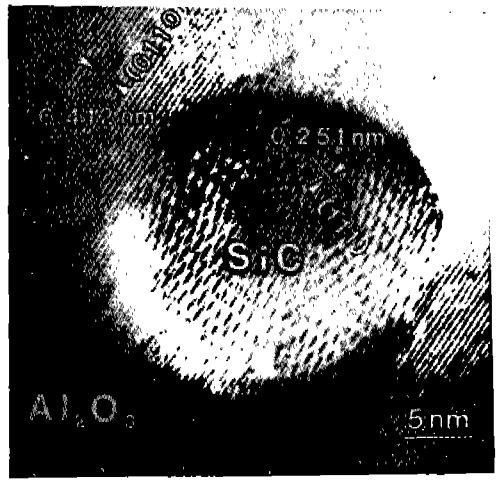


**Fig. 5. High resolution TEM picture of the $Al_2O_3$-SiC nanocomposite.**

that most of finer SiC particles, typically less that 0.2 μm, were predominantly dispersed within the $Al_2O_3$ grains and some larger particles at the grain boundaries. Similar observations on the second phase dispersion were also made for the MgO-SiC composites. High-resolution TEM observation revealed a notable fact that all the SiC particles within the $Al_2O_3$ grain were irregularly shaped. Fig. 5 show a typical high resolution TEM picture of the SiC particles within the $Al_2O_3$ grain. As is evident from Fig. 5, there was no obvious impurity phase at the interfaces. The interfacial particles also strongly bond the matrix/matrix interfaces in an $Al_2O_3$-SiC nanocomposite. This has been revealed by Ohji et al.[43] through estimation of equilibrium thickness of intergranular glassy film by force balance as well as direct observations using a HR-TEM in the previous study. This observation was also true for the MgO-SiC composites.[20]

## 3. Mechanical Properties

### 3.1. Fracture Strength and Toughness

The hardness, strength, and toughness tests of the $Al_2O_3$-SiC composites were made on the materials hot-pressed at 1,600℃, 1,700 and 1,800℃ for 5, 10, and 20 to 30 vol% SiC, respectively, which showed

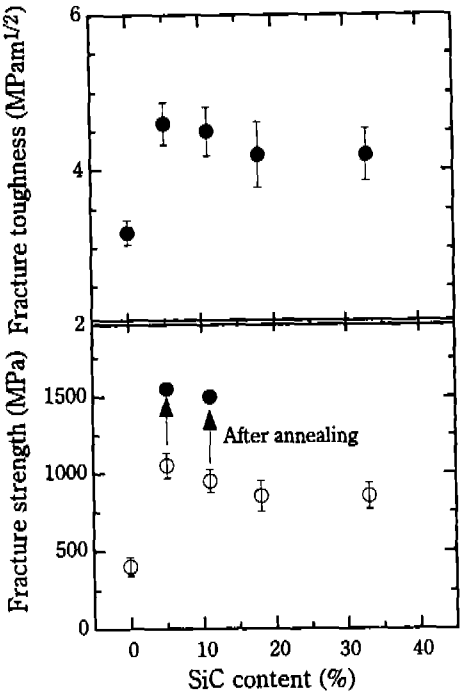


**Fig. 6. The variation of fracture strength and toughness of the $Al_2O_3$-SiC nanocomposites with the volume fraction of SiC.**

the nearly theoretical densities (over 99%) and were free from other impurity phases. For the MgO-SiC composites, the mechanical tests were performed for the materials hot pressed at 1900℃.

The variation of fracture strength and toughness of the $Al_2O_3$-SiC nanocomposites with the volume fraction of SiC is shown in Fig. 6. The strength increases tremendously from 355 to 1017 MPa with only 5 vol%SiC, and remains slightly-decreased strength 870 MPa up to 30 vol%SiC. The fracture toughness shows a similar trend in which the $K_{IC}$ values increases from 3.3 to 4.7 $MPam^{1/2}$ with 5 vol%SiC and keeps the constant value 4.4 $MPam^{1/2}$ up to 30 vol%SiC. The fracture strength of MgO was also improved from 330 to 700 MPa by incorporating 5 vol%SiC particles within the MgO grains, while the fracture toughness was increased from 1.7 to 2.3 $MPam^{1/2}$ with 5 vol%SiC. The higher toughness and strength approximately 5 $MPam^{1/2}$ and 750 MPa, were also observed for the MgO-30 vol%SiC composite, as shown in Fig. 7.

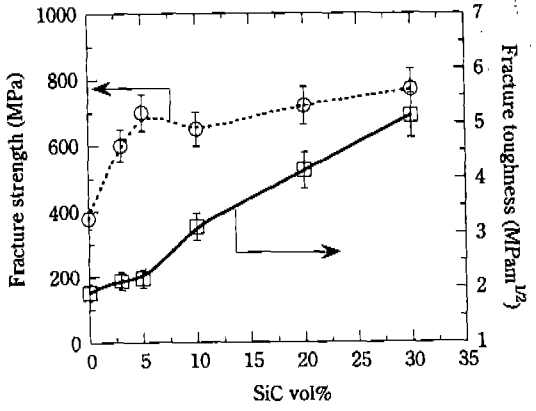


**Fig. 7. The variation of fracture strength and toughness of the MgO-SiC nanocomposites with the volume fraction of SiC.**

The fracture surface observation by SEM revealed that the second phase dispersions within the matrix grains changed the fracture mode from the intergranular to transgranular fracture. It may be thought that the change of fracture mode is caused by the tensile hoop stress of over 1,000 MPa around the inclusions within the matrix which is generated from the large thermal expansion mismatches. The high tensile stress will not produce the microcracks because the dispersed particle sizes are much smaller than the critical particle sizes for microcracking.[5,44] Thus, these composites may be toughened primarily by the crack bridging, although the possibility of stress induced microcrack toughening can not be completely ruled out, in special, for the MgO-SiC nanocomposite. The detail mechanisms will be discussed in Section 4.

The critical flaw sizes estimated from standard fracture mechanics relationship[5] using the above-mentioned data are about 9 μm for the monolithic MgO, which are almost equal to that for the 10 vol%SiC composite (10 μm). The strength increase at room temperature of MgO-SiC composites, therefore, will be attributed to the improved toughness by the SiC particles dispersed within the matrix grains. However, the notable strength improvement observed for the $Al_2O_3$-SiC composites (Fig. 6) can not be explained from

**Fig. 8. Sub-grain boundaries observed within the $Al_2O_3$ grains in the $Al_2O_3$-SiC nanocomposite.**

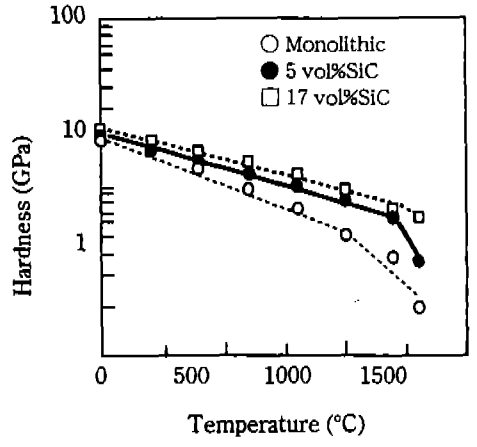


**Fig. 9. Temperature dependence of Vickers hardness for the $Al_2O_3$-SiC nanocomposites.**

only toughness increase. In the composite with 5 vol%SiC, the critical flaw size was decreased approximately from 23 to 6 μm. This remarkable decrease in critical flaw size is probably due to the refinement of matrix grains and/or the compressive stress (over 1, 500 MPa) around the SiC particles which prohibits the grain boundary fracture of the matrix during cooling from the fabrication temperatures.[5,13]

Fig. 8 shows the sub-grain boundaries observed in the $Al_2O_3$-SiC nanocomposites. These sub-grain boundaries were found to form due to intragranular hard SiC particles and pile-up of dislocations. These were generated in the $Al_2O_3$ matrix during cooling down from sintering temperatures by the highly-localized thermal stresses within and/or around SiC particles caused from the thermal expansion mismatch between $Al_2O_3$ and SiC. Therefore, it may be concluded that the observed refinement of matrix $Al_2O_3$ grains by the SiC dispersions is associated with this sub-grain boundary formation in the $Al_2O_3$ matrix grains. This mechanism will be discussed, in detail, in Section 5, and is considered to be partly true for the MgO-SiC nanocomposites.

### 3.2. High temperature Mechanical Properties

Fig. 9 gives the temperature dependence of Vickers hardness for the $Al_2O_3$-SiC nanocomposites. These composites exhibit higher hardness at all test temperature ranges and lesser degradation in hardness than that of monolithic $Al_2O_3$. Similar improvement of hot-hardness was observed for the MgO-SiC nanocomposites. Theses observed improvement of hardness degradation at the high temperatures suggests that the nano-size SiC particulate dispersed within $Al_2O_3$ and MgO grains prohibit the high temperature deformation and creep by the dislocation pinning with hard SiC particles.

Fig. 10 indicates the temperature dependence of the fracture strength for $Al_2O_3$-SiC and MgO-SiC com-

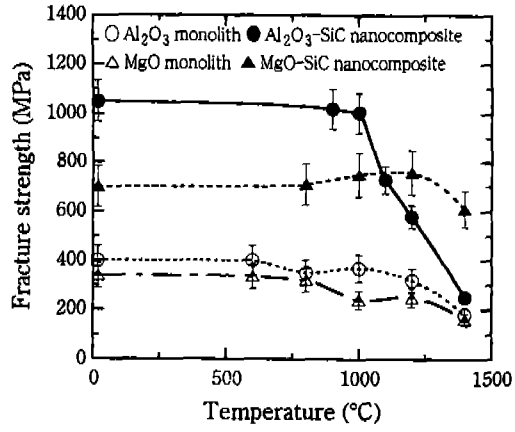


**Fig. 10. Temperature dependence of the fracture strength for the $Al_2O_3$-SiC and MgO-SiC nanocomposites.**

posites, respectively. The monolithic $Al_2O_3$ begins to exhibit significant reduction in strength above 1,000℃, whereas the $Al_2O_3$-5 vol%SiC composite keeps Its high strength up to 1,000℃. As is evident in Fig. 10, more notable improvement in high temperature strength is observed for the MgO-SiC nanocomposites. At the temperature range from 800 to 1,300℃, the MgO-SiC composites exhibit the considerably higher strength that that at room temperature.

It is well known that the grain boundary sliding and/or cavitation are responsible for the high temperature strength degradation of the oxide ceramics.[45] As above-mentioned, however, the dispersion of nano sized SiC within the matrix grains promote the transgranular fracture rather than intergranular. This phenomenon were also observed at the temperatures above 1,000℃. Thus, it may be concluded that the observed increase in strength at high temperatures is mainly due to the prohibition of the grain boundary sliding or cavitation by the dispersions within the matrix grains. In fact, the creep resistance is remarkably increased by inhibition of grain boundary sliding and cavitaion in $Al_2O_3$-SiC nanocomposites.[43] Another possible mechanism for the increased high temperature strength is the creep prohibition by the dislocation pinning with the fine dispersions within the matrix. This mechanism will be suggested by the fact that the MgO-SiC nanocomposites was significantly improved by inhibition of dislocation movement as well as grain boundary sliding.[46]

## 4. Strengthening and Toughening Mechanisms

### 4.1. Particle Bridging Toughening

The marked increase in strength for the $Al_2O_3$-SiC nanocomposite may be simply interpreted by the dispersed SiC nano-sized particles limiting the size of initial flaw. The dispersion of SiC particles into $Al_2O_3$ matrix, however, causes internal thermal tension in the matrix, and the fracture toughness should be lower than that of the monolith. This is inconsistent with the observed results; the toughness of $Al_2O_3$-SiC nanocomposite increased although the degree was modest. Thus, a certain toughening mechanism should operate in this composite. Ohji et al.[47] provided an evidence that the SiC nano-sized particles can bridge the crack in the vicinity behind the tip rather than deflection or bowing as a toughening mechanism in the $Al_2O_3$-SiC nanocomposites. On the basis of these observations, we here intend to estimate the toughness increase by the particle bridging, using a crack face shielding concept model.[48,49]

In this section we combine the toughness increase induced by the particle bridging and the toughness reduction caused by the residual thermal tension, to describe the particle volume fraction and size dependencies of the net fracture toughness. Fig. 11 shows the volume fraction dependencies of the bridging induced toughness increase, the residual tension induced toughness reduction, and the combined net toughness.

The particle diameter is fixed at 50 nm. $\Delta a$, $\Delta T$, $E_m$, $E_p$, $\upsilon_m$, and $\upsilon_p$ are taken as $3.8\times10^{-6}$/℃, 1,400℃, 380 GPa, 690 GPa, 0.25 and 0.23, respectively. With in-

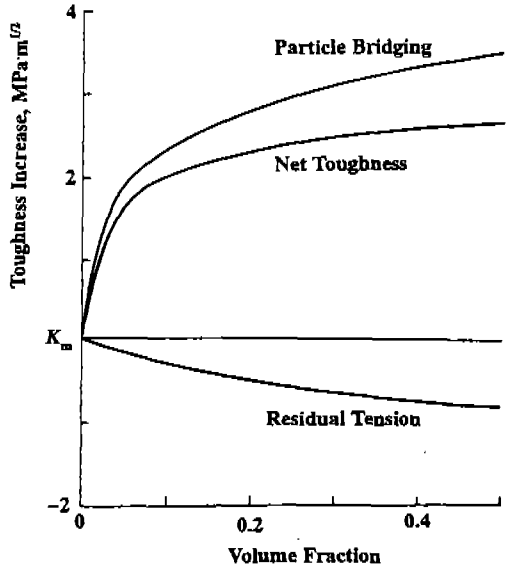


**Fig. 11. Volume fraction dependencies of the bridging-induced toughness increase, the residual-tension-induced toughness reduction, and the combined net toughness. The particle diameter is 50 nm.**

creasing the volume fraction, the both effects of the particle bridging and residual tension increase; however, the bridging-induced toughness increase in the range below 10 vol%, is steeper than that in the remaining range. This is explicitly due to the effects of crack propagation through the nearest neighbor particles. On the other hand, the toughness decrease by the residual tension is monotonous over the total range. Consequently the net toughness rises about 2 $MPam^{1/2}$ at 10 vol%, showing moderate increase in the remaining range for both cases. Fig. 12 shows the particle diameter dependencies of the two effects and the net toughness. The volume fraction is fixed at 5%. With increases in d, the toughness increases quite steeply below 100 nm, and moderately above that value. The toughness reduction caused by residual tension is again monotonous. The net toughness shows the almost plateau level at diameters above 100 nm.

The results of the present analyses qualitatively agree with the experimental results reported by Niihara et al.[16-19, 50] in general. For example, it has been shown that the toughening arises by dispersing a very small volume fraction, like 5 vol%, of the particles. The addition of nano-sized particles also has proved to be sufficiently effective for toughening. The model, however, predicts toughness increase of 2 $MPam^{1/2}$ at $f$p=5 vol% and $d$=50 nm, which is higher than any reported toughness-increases for $Al_2O_3$-SiC nanocomposite with similar volume fraction and particle size.[13)] That discrepancy exists partly because the present models assumed ideal cases. For example, all the doped particles were presumed to participate in crack bridging, which is not true particularly at the large volume fractions. The extremely high increases in fracture toughness at the large volume fractions, estimated in Fig. 11, therefore are not realistic.

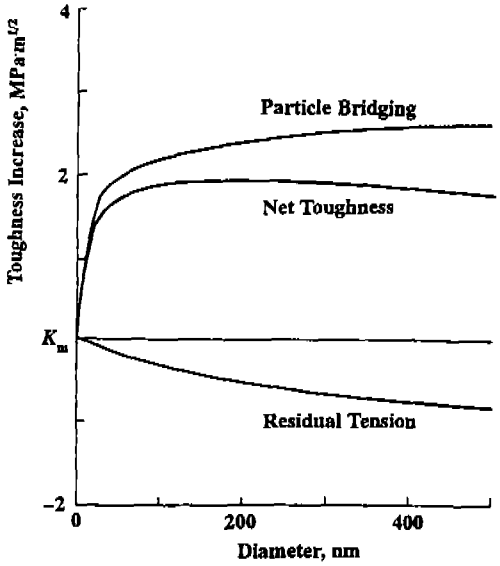


**Fig. 12. Particle diameter dependencies of the bridging-induced toughness increase, the residual-tension-induced toughness reduction, and the combined net toughness. The volume fraction is 0.05.**

### 4.2. R- Curve Behaviors and Strength

The toughness increases of the $Al_2O_3$-SiC nanocomposite are not remarkable as experimentally reported in other studies and analytically shown here. The benefit of the nanocomposite, however, lies in the steep rise of the fracture resistance in a very small crack extension.[47)] Since the particle bridging can operate within a matrix grain, the fracture toughness can be raised very steeply to a plateau level in a small crack extension. The crack extension distance required to attain the plateau toughness is equivalent to $l$ s which is a few hundred nano-meters.

Particle bridging does not operate in the case of a pre-existing flaw. Before the crack tip meets the particle to bridge it, the toughness is reduced by the matrix residual tension. When $f$p=5 vol% and $d$=100 nm, the toughness reduction is 0.3 $MPam^{1/2}$, and the toughness at this point becomes 2.7 $MPam^{1/2}$ assuming Km=3 $MPam^{1/2}$. (Note that this toughness value is in the case of the average matrix tension. A crack meeting particles should receive the residual tension at the interfaces, which is much higher than the mean value, leading to a lower toughness. Furthermore, intra-grain residual traction caused by crystallographic anisotropy, 100 MPa, is neglected.) On the other hand, the plateau toughness is about 5 $MPam^{1/2}$. The fracture resistance rises from about 2.7 $MPam^{1/2}$ to 5 $MPam^{1/2}$ in the a few hundred nano-meter crack ex-

tensions.

Bennison and Lawn[51,52] proposed an analytical approach to describe R-curve behavior of a non-transforming ceramics by considering grain bridging and pulling-out as the primary toughening mechanisms. Following their approach, we here estimate a rough outline of *R*- curve behavior for a monolithic $Al_2O_3$ polycrystalline. Similarly to their case study on an $Al_2O_3$, 2.5 $MPam^{1/2}$ is taken for the grain boundary fracture toughness. Assuming that the grain size is 2 μm which is a normal grain size of the most common $Al_2O_3$-SiC nanocomposite, and that the grain boundary residual traction caused by crystallographic anisotropy of individual grains is 100 MPa[53] the initial toughness without the effects of grain bridging and pulling-out can be estimated to be 2.3 $MPam^{1/2}$. The shielding zone length and plateau toughness also can be determined as about 300 μm and 3.3 $MPam^{1/2}$, respectively. This indicates that the fracture resistance increases from 2.3 to 3.3 $MPam^{1/2}$ over a 300 μm crack extension.

The fracture resistance curves (*R*-curves) for these two cases are compared schematically in Fig. 13,

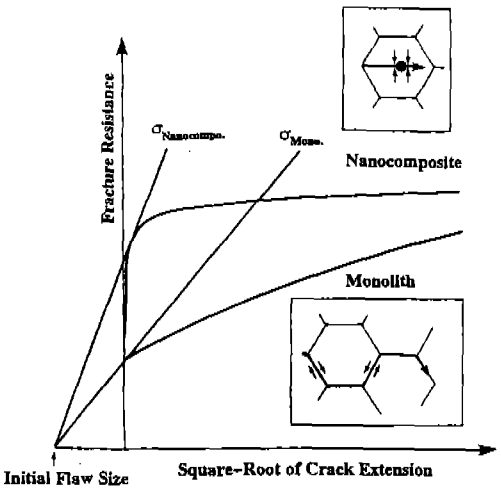


**Fig. 13. Schematic of fracture resistance curves of the $Al_2O_3$-SiC nanocomposite and monolithic $Al_2O_3$ polycrystal. Toughening of the monolith, being due to grain bridging and pulling-out, microcracking, etc., requires about 300 μm crack extension. The particle bridging operates inside a grain in the nanocomposite, the fracture resistance steeply rises in the 200-300 nm crack extension.**

where the crack extension is plotted to the right and the initial crack length is to the left in the abscissa, with the energy release rate in the ordinate. It is assumed that the $Al_2O_3$/SiC nanocomposite contains an initial crack with the same size as that of the monolithic $Al_2O_3$. Consider a penny-like crack in mode I loading as a fracture mechanics model. Supposing that the fracture strength of the monolithic $Al_2O_3$ is 500 MPa and the toughness is 2.5 $MPam^{1/2}$, the radius of the crack can be given as 20 μm, which is taken as the initial crack length. (The same initial crack length is assumed for the two materials, though it might be limited by the dispersed particles in the nanocomposite.) The strength can be determined by the slope of the tangent line from the initial crack length to the respective rising R-curves. For the case of the monolithic $Al_2O_3$, the R-curve behavior has made little contribution on catastrophic fracture, since a crack extension of a few hundred microns is required to obtain a substantial increase of fracture resistance. Note that a value measured in general fracture toughness tests, where a crack longer than several hundred microns is normally employed, is the plateau toughness after a sufficient crack extension. On the contrary, the steep rise of fracture resistance in the nanocomposite, should lead to an increase in the catastrophic failure strength. In other words, strength and toughness are compatible in this case.

Another benefit brought by the steep R-curve is that the strength distribution can be narrower resulting in a higher Weibull modulus. It is well known that, if the flaws involved in strength determination exhibit rising R-curve behavior, the Weibull modulus substantially increases.[54-56] In actuality, the markedly improved Weibull modulus has been reported for an $Al_2O_3$-SiC nanocomposite.[16] In summary, although the difference of the plateau fracture toughness is small between an $Al_2O_3$-SiC nanocomposite and monolithic $Al_2O_3$, the large difference exists in the R-curve behavior within a short crack-extension range, which controls the fracture strength. This difference can clearly interpret the observation in the $Al_2O_3$/SiC

nanocomposite; the addition of SiC nano-sized particles causes the vast increase in the strength and modest increase in the toughness.

### 4.3. Flow stress and dislocation interaction

In general, fracture may be initiated either at a flaw present before stressing, or at a flaw produced during stressing, i.e. initiated by dislocation motion. The original flaw sizes have been determined for each surface condition and the stress for their extension can be calculated, provided that the appropriate $\gamma_I$ values are known. A comparison of this stress with the measured surface and flow stresses enables the particular crack initiation mechanism to be identified.

The fracture strength increases with decreasing grain size both for monolithic MgO and MgO-SiC nanocomposites but the strength of the latter is substantially higher (Fig. 14). For the monolithic MgO, the fracture strength extrapolates to the flow stress at infinite grain size. This suggests strongly that fracture in this material is initiated from flaws produced by plastic flow. The fracture strength for MgO-SiC nanocomposites is several times higher than the flow stress, $\sigma_0$ a same fracture initiation process must be operating.

The fracture strength ($\sigma_f$) of MgO based ceramics will be given by the following functions[57,58] ;

$$\sigma_f=\sigma_0+k/d^{0.5} \quad (1)$$

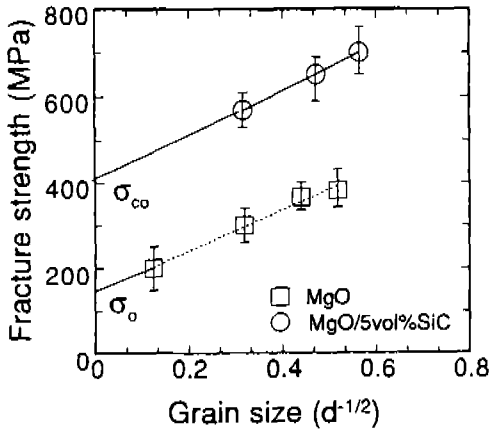


**Fig. 14. Grain size dependence of fracture strength for monolithic MgO and MgO-SiC nanocomposites.**

where $\sigma_0$ is the lattice friction stress for slip and independent of grain-size, and d is the grain or cell size controlling the slip band length.

A mechanism which can contribute to the strengthening of this composite system, is the increase of flow stress so caused by the dispersion of finer SiC particles within the MgO matrix grains. The bending strength as a function of grain size on $d^{-1/2}$ axis is plotted in Fig. 14 for monolithic MgO and MgO-5 vol%SiC nanocomposites. The fracture stress decreases with an increase in grain size and a linear relationship extrapolating to 150 MPa at infinite grain size is obtained. This suggests that the fracture is initiated from flaws produced by plastic flow as reported by Evans et al.[59] This value is almost same as reported value (180 MPa). They also investigated the flow stress of MgO with a higher concentration impurity within the grains using the indentation wing technique.[60] They found that the MgO material containing impurities exhibited higher flow stress than that for fully dense and pure MgO material. A similar increase in flow stress must be expected for the MgO-SiC nanocomposites, and a linear relationship extrapolating to about 400 MPa at infinite grain size is obtained for MgO-SiC nanocomposites.

When a moving dislocation encounters inclusions it will not, in general, be able to cut through them because the inclusions are generally stronger than the matrix. Consequently, the dislocation will have to bow between the inclusions and around them, leaving a dislocation loop around the particle, The stress required for this process is approximately.[61]

$$\tau_p=0.84 \cdot \mu b/l \quad (2)$$

where $l$ is the distance of closest approach between the particles: i.e. the bowing of the dislocation between the dispersions is exactly analogous of the dislocation segment. When fine dispersions are present, very large stresses must be applied before dislocation motion can occur, and the material exhibits a high strength.

The presence of SiC particles in MgO provides

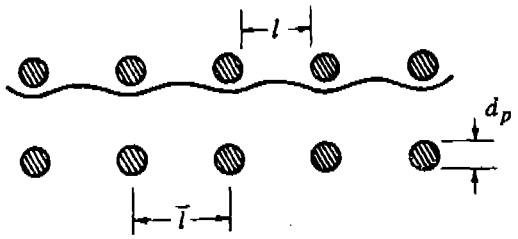


**Fig. 15. Illustration of the spacing between the particles and particle size.**

dispersion strengthening through the mechanism of direct dislocation-particle interactions. The spacing between the SiC particles in the slip plane can be computed with reference to the accompanying Fig. 15. The flow stress of pure polycrystalline MgO is $\sigma_0$ =180 MPa. The flow stress of 5 vol%SiC dispersed composite in the form of inclusion would be estimated. For MgO, shear modulus $\mu$=130 GPa and Burgers vector b=0.420 nm.

$$\text{Particle volume fraction=area fraction}=(\pi d_p^2/4)/\bar{l}^2 \quad (3)$$

$$\sigma_{0c}=\sigma_0+2\tau_p=\sigma_0+2\cdot 0.84\cdot \mu b/\bar{l} \quad (4)$$

From theses equations, the flow stress, $\sigma_{0c}$, of MgO-SiC nanocomposites is about 390 MPa, and this value is similar to the fracture stress extrapolated value of about 400 MPa at infinite grain size. This suggests strongly that fracture in this material as well as monolithic MgO is initiated from flaws produced by plastic flow. Then the drastic increase in fracture strength for the "MgO-SiC nanocomposites" could be due to the increase in the flow stress by the finer/intragranular SiC dispersion. It is considered, therefore, that the grain boundary fracture induced by dislocation flow inhibited by the finer/intragranular SiC dispersion, which, in turn, induces the intragranular crack propagation. The propagated crack reacted with dislocation which existed within MgO grains and/or generated by dislocation. As a toughening mechanism of MgO-SiC nanocomposite system, therefore, the plastic deformation by dislocation in the crack tip when crack propagated is considered.[62] In addition, stress induced microcracking as a toughening also observed.

## 5. Formation of dislocation and/or sub grain boundary

In general, when an effective elastic stress exceeds the yield stress of a material, the material will undergo plastic deformation, such as dislocation, dislocation network, and sub-grain boundary, rather than remain in a purely elastic state. For mathematical simplicity, additional assumptions are made for the model on the plastic behavior of the matrix. We assume that the flow stress-strain behavior of the matrix phase is independent of the strain rate and also of the stress orientation. We adopt the Von Misess yielding criterion,[63] namely that yielding occurs when an equivalent stress $\sigma_e$ exceeds the yield stress $\sigma_y$, where s is given by

$$\sigma=\sigma_{\theta\theta}-\sigma_{rr} \quad (5)$$

Substitution of the tangential stress, $\sigma_{\theta\theta}$ and radial stress, $\sigma_{rr}$, into Eq. (5) yields $\sigma_e=(3/2)\ P_I\ (R/r)^3$ in the purely elastic state. Therefore, yielding will start at the matrix/particle interface when the stress $P_I$ reaches the critical value $2\ \sigma_y/3$. As the internal stress $P_I$ increases beyond the critical value, a plastic zone develops adjacent to the matrix/particle interface. The deformation of $\alpha$-$Al_2O_3$ has been studied under hydrostatic confining pressure at temperatures below the brittle to ductile transition temperature.[64] The temperature dependence of the critical reserved shear stress ($\tau_{crss}$) for both basal slip and prism plane slip over a large temperature range can be described by a simple logarithmic law,

$$\ln \tau_{crss}=\ln \tau_0-BT \quad (6)$$

where $\tau_0$ is the flow stress at 0 K, and B is constant, and both $\tau_0$ and B are lower for prismatic slip than for basal slip, making prismatic slip the easy slip system below 600℃, as shown in ref.[64] The stress relaxation becomes less active in pure $Al_2O_3$ as well as composite system as temperature decreases, when the driving forces (e. g. applied stress or residual stress due to the thermal expansion mismatch) are constant.

And though residual stress due to the thermal expansion mismatch exists in the composites, when the internal stress $P_I$ does not exceed the critical value for yield stress, a plastic zone cannot develop adjacent to the matrix/particle interface. Therefore, the relationship between the internal stress $P_I$ and residual stress must be discussed, where the yield stress and internal stress strongly depend upon the temperature. If the matrix is elastic, the stress in the spherical inclusion is hydrostatic and is given by internal stress, $P_I$. Applying the data of $Al_2O_3$ for matrix and those of SiC for inclusion into $P_I$, we obtain

$$P_I=1.287\Delta T \quad (7)$$

It shows that one-degree decrease in temperature will induce a compressive stress of about 1.3 MPa for $Al_2O_3$-SiC system, provided the matrix is the elastic limit. Correspondingly, the stress in the matrix can be expressed as eq. (8). Obviously, a decrease in temperature will induce a tensile stress in the matrix. The residual average microstresses also can be calculated from these internal stresses ($P_I$). The average microstresses in second phase, $\sigma_{As}$ are given by

$$\sigma_{As}=1.287(1-f_s)\,\Delta T \quad (8)$$

If we suppose that residual stress completely relaxes to a) 1,000℃ (relaxed temperature by grain boundary diffusion[65,66] which is main relaxation mechanism of $Al_2O_3$ monolith and microcomposites), b) 1,400 ℃ (relaxed temperature by lattice/grain boundary diffusion which is main relaxation mechanism of nanocomposites), and c) 1,700℃ (fabrication temperature: This means that nothing is relaxed), from fabrication temperature, the temperature dependence of internal stress and yield stress for different relaxation temperatures on $Al_2O_3$-SiC composite systems was obtained as shown in Fig. 16.

Fig. 16 shows the variance of equivalent and yield stresses with temperature which depend on SiC volume fraction and slip system, when residual stresses relax to (a) 1,000℃, (b) 1,400℃ and (c) 1,700℃, respectively.

The dislocation movement will start at the matrix/particle interface when the stress 3/2 $P_I$ reaches the yield stress $\sigma_y$. As the stress 3/2 $P_I$ increases beyond the yield stress, a plastic deformation develops adjacent to the matrix/particle interface, extending to a radius depending upon the magnitude of $P_I$. When

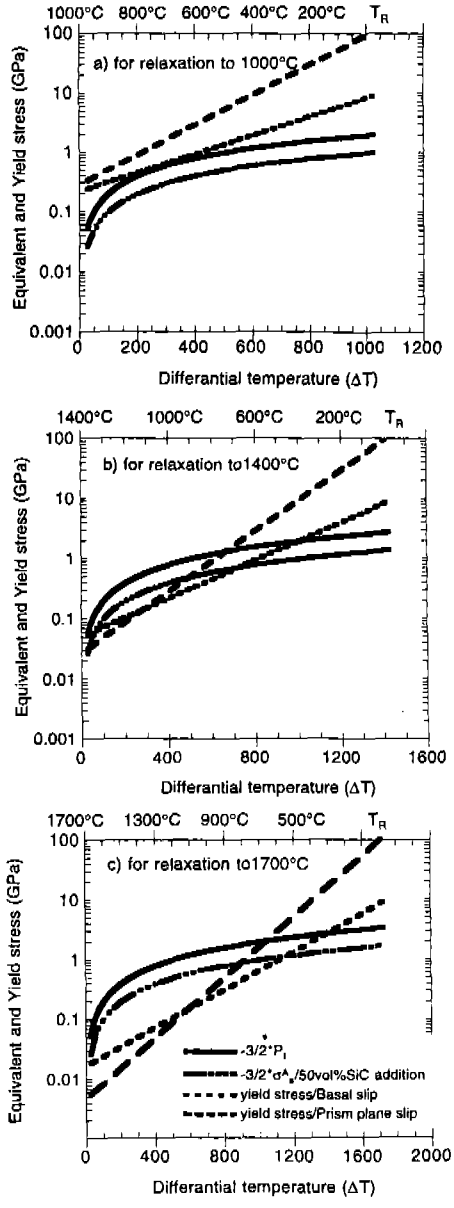


**Fig. 16. Variance of equivalent and yield stress with temperature which depend on SiC volume fraction and slip system, when residual stress relax to (a) 1,000 °C, (b) 1,400 °C and (c) 1,700 °C.**

the complete relaxation occurs to 1,000℃ (corresponding to $Al_2O_3$ monolith and microcomposites), the plastic deformation by the dislocation generation can not occur in prismatic slip and basal slip systems, because the residual stress term, 3/2 $P_I$ due to thermal mismatch is lower than the yield stress for the easiest slip system in $Al_2O_3$, over the whole temperature range as calculated in Fig. 16(a). Otherwise, if the complete relaxation occurs to 1,400℃ (corresponding to the nanocomposites and Fig. 16(b)), the plastic deformation by the dislocation generation can occur in prism plane slip and basal slip systems. Especially, for prism plane slip, the residual stress relaxation by the dislocation generation and movement reaches up to 500℃. It is worth to note that if the temperature for complete relaxation is higher, the relaxation by dislocation generation and movement continue to lower temperature. These results coincided that the higher internal stresses generated, during cooling down from stopping temperatures for the stress relaxation by lattice diffusion and the depressed diffusion in the matrix/second phase, induced the formation of dislocation both prism plane and basal plane for $Al_2O_3$-SiC nanocomposite system.[23] Also, these consequences well explained the microstructure of nanocomposites. This plastic deformation within the matrix grain due to residual stresses also was observed in MgO-SiC nanocomposite system.[21]

## 6. Remarks

The incorporation of nano-sized SiC particle into $Al_2O_3$ or MgO materials leads to a significant improvement in fracture strength and toughness and parallels the action of this type of SiC in improving other mechanical properties such as creep resistance, high temperature strength, and so on. Although grain size/critical flaw size is the single most important parameter in determining the strength at room temperature of polycrystalline oxide materials, the presence of nano-phase SiC has (at equivalent grain size) a significant additional beneficial effect as a toughening mechanism.

This review has revealed that the deagglomeration and homogeneity process of SiC nano-sized particles as well as oxide materials for the basic conventional processing route for $Al_2O_3$-SiC and MgO-SiC nanocomposite system, and the improvement of the mechanical properties could be rationalized by the following roles of the nano-size SiC particles dispersed within the matrix grains.

(1) The nano-size SiC particles restrain the grain growth of matrix and decrease the abnormal grain growth.

(2) The highly localized stresses within and/or around the SiC particles, which is produced from the thermal expansion mismatch between matrix and SiC, generate the dislocation during cooling from the fabrication temperatures. The nano-size SiC particles pin and pile-up the dislocations to make sub-grain boundaries within the matrix grains, which occur the refinement of matrix grains for strengthening.

(3) The localized tensile stress around the nano-size SiC particles induces the transgranular fracture, and then the toughening occurs due to the crack tip shielding by the SiC particles. The high temperature mechanical properties are also improved by the change of fracture mode, because the grain boundary effects on the high temperature mechanical properties are diminished.

The most interesting system for industrial application appears to be oxide based nanocomposites. It has been demonstrated that conventional powder processing in an aqueous medium, slip casting and pressureless sintering represents a promising processing route for nanocomposites. However, improved strengths have not been reported for pressureless sintered nanocomposites. The reason may be the higher porosity. These problems have been solved by applying the post-HIPing technique.[67]

Applying the concept of nanocomposites, several applications could be possible. The examples are functional nano-sized ceramic dispersed ceramic bas-

ed nanocomposite,[68,69] nano-sized metal dispersed ceramic based nanocomposite,[24-28] nano-sized ceramic particle dispersed metal based nanocomposite,[70] nano-sized ceramic dispersed nano-sized ceramic based nanocomposite,[71] and so on, which is to develop the multi-functional materials.

## References


1. R. P. Wahi and B. Ilschner: "Fracture Behavior of Composites Based on $Al_2O_3$-TiC", J. Mater. Sci., **15** (1980) 875.
2. F. F. Lange: "Transformation Toughening", J. Mater. Sci., **17** (1982) 225.
3. N. Claussen: "Strength Strategies for $ZrO_2$-Toughened Ceramics at High-Temperatures", Mater. Sci. & Eng., **71** (1985) 23.
4. F. F. Lange: "Strong High Temperature Ceramics", Ann. Rev. Mat. Sci., **4** (1974) 365.
5. K. Niihara, A. Nakahira, T. Uchiyama, and T. Hirai: "High Temperature Mechanical Properties of $Al_2O_3$-SiC Composites", pp. 103-116, in Fracture Mechanics of Ceramics, Vol 7, Edited by R. C. Bradt, A. G. Evans, D. P. H. Hasselman and F. F. Lange, Plenum, New York (1986).
6. A. Nakahira, K. Niihara, and T. Hirai: "Microstructure and Mechanical Properties of $Al_2O_3$-SiC Composites", Yogyo-Kyokai-Shi, **94** (1987) 767.
7. P. E. Becher and G. C. Wei: "Toughening Behavior in SiC whisker Reinforced Alumina", J. Am. Ceram. Soc., **67C** (1984) 267.
8. J. Homeny, W. L. Vaughn, and M. K. Ferber: "Processing and Mechanical Properties of SiC Whisker $Al_2O_3$ Matrix Composites", Amer. Ceram. Soc. Bull., **66** (1987) 333.
9. T. N. Tiegs and P. E. Becher: "Sintered $Al_2O_3$-SiC Whisker Composites", Amer. Ceram. Soc. Bull., **66** (1987) 339.
10. T. Nishida, T. Shiono, H. Yamauchi, and T. Nishikawa: "Fracture Energy of MgO-SiC Whisker Composite Ceramics", ZaiRyo, **36** (1987) 17.
11. T. Uchiyama, S. Inoue, and K. Niihara: "Multiple Toughening in $Al_2O_3$-SiC Whisker/ $ZrO_2$ Composites", pp. 193-200 in Silicon Carbide Ceramics, Edited by S. Somiya and K. Inomata, UchidaroKakuho, Tokyo, (1988).
12. K. Niihara: "New design concept of structural ceramics-ceramic nanocomposites", J. Ceram. Soc. Jpn., **99** (1991) 974.
13. A. Nakahira and K.Niihara: "Microstructures and fracture behaviors at high temperatures for $Al_2O_3$-SiC nanocomposites", In Fracture Mechanics of Ceramics, Vol. 9. ed. M. Sasaki, R. C. Bradt, D. P. H. Hasselman and D. Munz, Plenum press, New York, pp. 165-178 (1992).
14. T. Hirano and K. Niihara: "Microstructure and mechanical properties of $Si_3N_4$/SiC nanocomposites fabricated from amorphous Si-C-N precursor powders", Nanostruct. Mater. **5** (1995) 808.
15. T. Ohji, T. Hirano, A. Nakahira, and K. Niihara: "Particle/matrix interface and its role in creep inhibition in alumina/silicon carbide nanocomposites", J. Am. Ceram. Soc., **79** (1996) 35.
16. K. Niihara: "Ceramic Composites-nanocomposites", Electronic Ceramics, **9** (1988) 44.
17. K. Niihara and A. Nakahira: "Development of Strong $Al_2O_3$-SiC Composites", pp. 129-134 in Proc. of MRS meeting on a Advanced Materials, Plenum, Tokyo (1988).
18. K. Niihara: "Nanostructural Design and Mechanical Properties of Ceramic Composites", J. Jp. Soc. Powder and Powder Metallurgy, **37** (1990) 348.
19. K. Niihara and A. Nakahira: "Fabrication and Properties of Alumina Based Nanocomposites", pp. 128-138 in Proc. 7th Korea-Japan Seminar on New Ceramics (1990).
20. Y. H. Choa, S. Ueda and K. Niihara: "Effects of Second Phase Particles on Interface and Grain Boundary Structure in MgO-Based Ceramics", Ceramic Trans. **44** (1994) 417.
21. Y. H. Choa, T. Kusunose, A. Nakahira and K. Niihara: "Size Effects of Dispersion Phase on Residual Stresses in Oxide Based Nanocomposites", Proc. 4th International SAMPE Symposium, 400-406 (1995).
22. N. Bamba, Y. H. Choa and K. Niihara: "Fabrication and mechanical properties of nano-sized SiC particulate reinforced yttria stabilized zirconia composites", Nanostructured Material, **9** (1997) 497.
23. Y. H. Choa, A. Nakahira, T. Ohji, and K. Niihara: "Thermal Residual Stress Relaxation Behavior of Oxide Based Nanocomposites", J. Mater. Sci, in contribution.
24. T. Sekino, A. Nakahira, M. Nawa, and K. Niihara: "Fabrication of Al2O3/W nanocomposites", J. Jpn. Soc. Powder Powder. Metall., **38** (1991) 326.
25. M. Nawa, T. Sekino and K. Niihara: "Fabrication and mechanical behavior of Al2O3/Mo nanocomposites", J. Mater. Sci., **29** (1994) 3185.
26. T. Sekino, T. Nakajima, S. Ueda, and K. Niihara: "Reduction and sintering of a nickel-dispersed-alumina composite and its properties", J. Am. Ceram. Soc., **80** (1997) 1139.
27. T. Sekino and K. Niihara: "Microstructural characteristics and mechanical properties for $Al_2O_3$/metal

nanocomposites", Nanostruct. Mater., **6** (1995) 663.
28. M. Nawa, K. Yamazaki, T. Sekino, and K. Niihara: "Microstructure and mechanical behavior of 3Y-TZP/Mo nanocomposites possessing a novel interpenetrated intragranular microstructure". J. Mater. Sci., **31** (1996) 2849.
29. A. Nakahira, H. Tamada, and K. Niihara: "Microstructure and mechanical properties of Ti-Al based composites", J. Jap. Soc. Powder Powder Metall., **41** (1994) 514.
30. Y. Suzuki, T. Sekino, and K. Niihara: "Effects of $ZrO_2$ addition on microstructure and mechanical properties of $MoSi_2$", Scripta Metall. et Mater., **33** (1995) 69.
31. M. Okuyama, G. J. Garvey, T. A. Ring, and J. S. Haggerty: "Dispersion of Silicon Carbide Powders in Nonaqueous Solvents", J. Am. Ceram. Soc., **72**(10) (1989) 1918.
32. M. S. Kaliszewski, and A. H. Heuer: ""Alcohol Interaction with Zirconia Powders", J. Am. Ceram. Soc., **73**(6) (1990) 1504.
33. H. K. Varma, T. V. Mani, A. D. Damodaran, K. G. Warrier, and U. Balachandran: "Characteristics of Alumina Powder Prepared by Spray-Drying of Boehmite Sol", J. Am. Ceram. Soc., **77**(6) (1994) 1597.
34. R. T. Morrison and R. N. Boyd: "Organic Chemistry", p 563, Six Edition, Published by Prentice-Hall (1992).
35. R. G. Horn, "Surface Forces and Their Action in Ceramic Materials", J. Am. Ceram. Soc., **73**(5) (1990) 1117.
36. S. Mitzuta, W. R. Canon, A. Bleier, and J. S. Haggerty: "Wetting and Dispersion of Silicon Powder without Deflocculants", Am. Ceram. Soc. Bull., **61**(8) (1982).
37. S. Wada: "Increase of Oxygen Content in $Si_3N_4$ Powder during Ball Milling Using Alcohol as Solvent", J. Ceram. Soc. Jp., **104**(11) (1996) 1085.
38. T. Hirano, J. Yang, and K. Niihara: "Effects of Ball-Milling Time on the Properties of Low Purity β-hase Silicon Nitride Powder and the Hot-Pressed Body", J. Ceram. Soc. Jp., **104**(4) (1996) 348.
39. F. W. Dynys and J. W. Halloran: "Reactions During Milling of Aluminum Oxide", J. Am. Ceram. Soc., **64** (1981) C62.
40. M. J. Readey, R. R. Lee, J. W. Halloran, and A. H. Heuer: "Processing and Sintering of Ultrafine MgO-$ZrO_2$ and (MgO, $Y_2O_3$)-$ZrO_2$ Powders", J. Am. Ceram. Soc., **73**(6) (1990) 1499.
41. M. E. Winfield, "Catalytic Dehydration and Hydration" p. 103 in Catalysis, Vol VII. Edited by P. H. Emmett. Reinhold Publishing Corp., New York (1960).
42. Y. H. Choa, N. Bamba, and K. Niihara: "Effect of Pure Solvents without Deflocculants for Finer SiC Particle Dispersed MgO Based Composite", J. Mater. Sci, in contribution.
43. T. Ohji, A. Nakahira, T. Hirano and K. Niihara: "Tensile Creep Behavior of Alumina/Silicon Carbide Nanocomposite", J. Am. Ceram. Soc., **77**(12) (1994) 3259.
44. J. Selsing: "Internal Stress in Ceramics", J. Am. Ceram. Soc., **44** (1961) 419.
45. A. G. Evans and W. Blumenthal: "High Temperature Failure in Ceramics", pp. 423-448, in Fracture Mechanics of Ceramics, Vol 6., Edited by R. C. Bradt, A. G. Evans, D. P. H. Hasselman and F. F. Lange, Plenum, New York, (1983).
46. E. Yasuda, Q. BaO. and K. NIIhara: "The effects of fIne SIC partIcles on the creep of MgO at hIgh temperatures", J. Ceram. Soc. Jpa., **100** (1992) 514.
47. T. Ohji, Y. H. Choa, and K. Niihara: "Strengthening and Toughening Mechanisms of Ceramic Nanocomposite", J. Am. Ceram. Soc. in print.
48. D. S. Dugdale: "Yielding of Steel Sheets Containing Slits", J. Mech. Phys. Solid, **8** (1960) 100.
49. G. I Barenblatt: "Mathematical Theory of Equilibrium Cracks in Brittle Fracture," Advan. Appl. Mech., **7** (1962) 55.
50. K. Niihara and A. Nakahira, and T. Hirano: "Particulate Strengthened Ceramics, Nanocomposites", Presented at US/Japan Workshop on the Processing of Advanced Ceramics, Sheattle, Aug. 21-24 (1988).
51. S. J. Bennison and B. R. Lawn: "Role of Interfacial Grain-Bridging Sliding Friction in the Crack Resistance and Strength Properties of Nontransforming Ceramics", Acta Metall., **37**(10) (1989) 2659.
52. S. J. Bennison and B. R. Lawn: "Flaw Torelance in Ceramics with Rising Crack Resistance Characteristics", J. Mater. Sci., **24** (1989) 3169.
53. J. E. Blendelland R. L Coble: "Measurement of Stress Due to Thermal Expansion Anisotropy in $Al_2O_3$", J. Am. Ceram. Soc., **65**(3) (1982) 174.
54. K. Kendall, N. McN. Alford, S. R. Tan, and J. D. Birchall: "Influence of Toughness on Weibull Modulus of Ceramic Bending Strength", J. Mater,Res., **1**(1) (1986) 120.
55. R. F. Cook and D. R. Clarke: "Fracture Stability, R-Curves and Strength Variability", Acta metall., **36**(3) (1988) 555.
56. D. K. Shetty and J.-S. Wang: "Crack Stability and Strength Distribution of Ceramics That Exhibit Rising Crack Growth Resistance (R-Curve) Behavior", J.Am. Ceram. Soc., **72**(7) (1989) 1158.
57. B. J. Dagleish, P. L. Pratt, R. D. Rawlings and A. Frakhrr: Mater. Sci. Eng., **45** (1980) 9.
58. R. J. Stokes and C. H. Li: J. Am. Ceram. Soc., **46** (1963) 423.
59. A. G. Evans and R. W. Davidge: Phil. Mag., **20** (1969). 373.

60. A. G. Evans, D. Gilling and R. W. Davidge: J. Mater Sci., **5** (1970) 187.
61. E. Arzt and D. Wilkinson: Acta. Tetall, **34** (1986) 1893.
62. Y.H. Choa, M. V. Swain, and K. Niihara, in preperation.
63. G. E. Dieter, Mechanical Metallurgy, McGraw-Hill, New York, NY (1961).
64. K. Peter, D. Lagerlof, A. H. Heuer, J. Castaing, J. P. Riviere and T. E. Mitchell: "Slip and Twining in Sapphire($\alpha$-$Al_2O_3$)", J. Am. Ceram. Soc., **77**(2) (1994) 385.
65. Z. Li and R.C. Bradt: "Micromechanical Stress in SiC-Reinforced Al2O3 Composites", J. Am. Ceram. Soc., **72**(1) (1989) 70.
66. A. Abuhasan, C. Balasingh, and P. Predecki, J. Am. Ceram. Soc., **73**(8) (1990) 2474.
67. M. Ishituka and M. Tamai, "Fabrication and Mechanical Properties of Pressureless Sintered $Al_2O_3$/SiC Nanocomposites", J. Jpn. Soc. of Powd. and Powd. Metal., **39** (1992) 1109.
68. T. Nagai, H. J. Hwang, M. Yasuoka, M. Sando and K. Niihara: "Dielectric Properties of Ceramic Nanocomposite with $BaTiO_3$ Dispersoid", Ceramic Transactions, vol 85, (Innovative Processing and Synthesis of Ceramics, Glasses, Composites, Edited by N. P. Bansal, K. V. Logan and J. P. Singh. America Cermic Society, Westervill, OH, 1997), in print.
69. T. Nagai, H. J. Hwang, M. Sando and K. Niihara: "jPreparation of Ceramic Nancomposite with Perovskite Dispersoid", Mater. Res. Soc. Symp. Proc., vol 457, (Nanophase and Nanocomposite Materials II, Edited by S. Komarneni, J. C. Parker and H. J. Wollenberger, Materials Research Society, Pittsburgh, PA, 1997), in print.
70. T. Yamamoto, R. D. Shull, P. R. Bandaru, F. Cosandey, H. W. Hahn: "Superparamagnetic Nanocomposite of Silver/Iron-Oxide by Inert Gas Condensation", Jpn. J. Appl. Phys. 33, L 1301-L 1303, Part 2, No. 9B (1994).
71. M. Yoshimura, Y. H. Choa, and T. Sekno, and K. Niihara: "Fabrication and Properties of Nano-Structured Oxide Ceramics", Proc. of 6th Int. Sym. on Ceramic Materials & Components for Engines, Arita, Jan (1997), in print.